



# Automatic Striatal ROI Delineation for Semi-quantitative Analysis of $^{99m}\text{Tc}$ -TRODAT-1 Brain SPECT Imaging

Bang-Hung Yang<sup>1,2</sup> · Kang-Ping Lin<sup>3,4</sup> · Mei-Fen Chen<sup>3,4</sup> · Jui-Hung Weng<sup>5</sup> · Pan-Fu Kao<sup>5</sup> · Wen-Chen Lin<sup>3,4</sup> · Ren-Shyan Liu<sup>1,2,6</sup>

Received: 6 December 2019 / Accepted: 7 May 2020 / Published online: 14 May 2020  
© Taiwanese Society of Biomedical Engineering 2020

## Abstract

**Purpose** Single-photon emission computed tomography (SPECT) imaging, a relatively inexpensive nuclear imaging technique, has been used as a diagnostic tool for Parkinson's disease (PD). The tracer  $^{99m}\text{Tc}$ -TRODAT-1 is commonly used in Taiwan, where the imaging cost is covered under the national health insurance system. However, poor TRODAT-SPECT imaging resolution is a problem. Therefore, we developed a semi-quantitative program that can perform automatic region of interest (ROI) delineation for semi-quantifying striatal dopamine transporter activities.

**Methods** A total of 228 subjects were enrolled in this study, including PD patients ( $n=62$ ) and healthy controls ( $n=166$ ). The subjects received a  $^{99m}\text{Tc}$ -TRODAT-1 brain SPECT scan. Some of the subjects ( $n=40$ ) also received a high-resolution magnetic resonance imaging (MRI) scan for the evaluation of the accuracy of the semi-quantitative assessment. In addition, the developed automatic ROI delineation method was used to calculate the striatal specific uptake ratio (SUR) in dopamine transporter imaging. The reproducibility of the SUR obtained using the method was compared to those in previous studies.

**Results** Based on linear regression analysis ( $r^2=0.92$ , correlation coefficient=0.96), a correlation was found between the results obtained using the automatic ROI delineation method and those of the manual method in striatum with the corresponding MR images. The age-related decline of SUR availability measured in this study was 6.4% per decade. There was almost no difference between our results and those in related clinical studies.

**Conclusions** The proposed automatic ROI delineation program for SUR analysis was tested and used to estimate the ROIs in TRODAT-SPECT images to aid PD diagnosis. The program could be helpful for physicians who are inexperienced with TRODAT-SPECT images.

**Keywords** Automatic ROI delineation · Specific uptake ratio analysis · SPECT imaging · Parkinson's disease

## Abbreviations

%AI	Percentage of the asymmetry index
DAT	Dopamine transporter
HYS	Hoehn and Yahr scale
MFC	Microsoft foundation classes
MRI	Magnetic resonance imaging
PD	Parkinson's disease
PET	Positron emission tomography
ROI	Region of interest
SPECT	Single-photon emission computed tomography
SPM	Statistical parametric mapping
SUR	Specific uptake ratio
$\text{SUR}_{\text{left}}$	The average values of the ROI striatum on the left sides
$\text{SUR}_{\text{right}}$	The average values of the ROI striatum on the right sides

✉ Wen-Chen Lin  
lin\_wenchen@cycu.org.tw

<sup>1</sup> Department of Biomedical Imaging and Radiological Sciences, National Yang-Ming University, Taipei, Taiwan

<sup>2</sup> Department of Nuclear Medicine and National PET/Cyclotron Center, Taipei Veterans General Hospital, Taipei, Taiwan

<sup>3</sup> Technology Translation Center for Medical Device, Chung-Yuan Christian University, Taoyuan, Taiwan

<sup>4</sup> Department of Electrical Engineering, Chung-Yuan Christian University, Taoyuan, Taiwan

<sup>5</sup> Department of Nuclear Medicine, Chung Shan Medical University Hospital, Taichung, Taiwan

<sup>6</sup> Department of Nuclear Medicine, Cheng Hsin General Hospital, Taipei, Taiwan

## 1 Introduction

The diagnosis and treatment of idiopathic Parkinsonism require experienced clinicians to provide clinical consultation and neuroscience examination [1–3]. The movement disorders of patients must also be examined for accurate diagnosis. However, the symptoms in the early stage of Parkinson's disease (PD) are mild. When obvious movement disorders appear, more than 80% of the dopaminergic nerve system in the patient's brain has often already been damaged [4, 5]. Nuclear medicine dopamine imaging is a tool for the early diagnosis of idiopathic Parkinsonism [6]. The dopamine transporter (DAT) is a specific protein on dopaminergic neurons. With neurodegeneration, the number of DATs decreases. Dopamine imaging is applied to assess the number of striatal dopaminergic neurons in the brain by marking the dopamine system with nuclear medicine. The images can be used by clinicians to determine whether movement disorders are caused by dopaminergic neurodegeneration. Different types of Parkinsonism require different treatments and prognoses. Examples include vascular Parkinsonism, which is caused by a continuous mild stroke near the basal ganglia, which controls movement, and manganese-induced Parkinsonism. Therefore, it is very important to effectively distinguish idiopathic Parkinsonism from other types of Parkinsonism. Early and correct diagnosis of idiopathic Parkinsonism is very important for clinicians because adequate treatments can slow the deterioration caused by the disease and maintain the quality of life of the patient [7].

Dopamine imaging such as TRODAT-SPECT (single-photon emission computed tomography) or FDOPA-PET (positron emission tomography) is used to accurately distinguish different types of Parkinsonism [8]. Traditionally, diagnosis based on dopamine imaging with SPECT relies on professional clinicians to realign the imaging and assess whether the striatum function is degraded. Clinicians must also perform a semi-quantitative analysis to calculate the specific uptake ratio (SUR). To calculate the SUR, a region of interest (ROI) on the outside of both striatum is circled, and an area (such as the cerebellum or occipital lobe) is also circled for the reference. The ROI must be circled one by one on several tomographic images, which is laborious and subject to human error [9].

A SPECT scanner is less expensive than a PET scanner and thus an examination with TRODAT-SPECT is less expensive than that with FDOPA-PET [10, 11]. Many research teams have developed SPECT automatic semi-quantitative analysis tools for evaluating the striatal uptake of dopamine transporters [12–21]. Nevertheless, automated analysis may be inaccurate for SPECT imaging that uses different acquisition protocols and reference values

from those in the normal control database. In Taiwan,  $^{99m}\text{Tc}$ -TRODAT-1 is covered under the national health insurance. An automatic, fast, and reliable method for automatic semi-quantitative TRODAT-SPECT dopamine scanning to help clinicians diagnose Parkinson's disease is required. A program that can effectively assist the early stage diagnosis of Parkinsonism is urgently required. The present study proposes an automatic semi-quantitative analysis program for  $^{99m}\text{Tc}$ -TRODAT-1 SPECT scanning. This program provides an accurate semi-quantitative SPECT dopamine imaging analysis report.

An important step in DAT semi-quantification is the correct delineation of the ROI in SPECT images. This study evaluates the feasibility of the proposed automatic striatal ROI delineation method. The semi-quantitative data obtained using the automatic ROI delineation are compared with those from manual ROI delineation in SPECT images guided by MRI. The correlations between the SUR and age-related decline in health controls, and those between SUR, asymmetry index, and PD stage are examined.

## 2 Materials and Methods

### 2.1 Automatic Semi-quantitative Analysis Program

The automatic analysis consists of four main steps. Figure 1 shows the entire process of the proposed method. First, the raw reconstructed SPECT images are spatially resampled to obtain a  $1\text{ mm}^3$  resolution. Second, four ROIs with fixed dimensions are set corresponding to the left and right striatum. Third, the mean value of counts in each ROI is calculated to obtain the SUR. Finally, the resulting parameters are collected as a report. The automatic ROI delineation on the striatum is discussed in detail below.

#### 2.1.1 Automatic ROI Delineation on Striatum

The structural and functional mapping of the brain is a major approach in neuroscience. To properly set the ROI on the caudate and putamen, the relative brain size must be measured based on the head size of the subject. The proposed automatic ROI delineation method is as follows:

**2.1.1.1 Slice Selection for Processing** With images resliced at a resolution of  $1\text{ mm}^3$ , a SPECT scan consists of 256 transaxial slices from the top to bottom of the head. The summed SPECT scan image is calculated along the sagittal and coronal planes of all slices to decide the “Up” index and the “Down” (DW) index for the brain. The horizontal projection profile is obtained by summing pixel values from the summed SPECT scan image. The lowest value of the upper part in the profile is detected as “Up” index. Besides,

**Fig. 1** Scheme of the proposed method

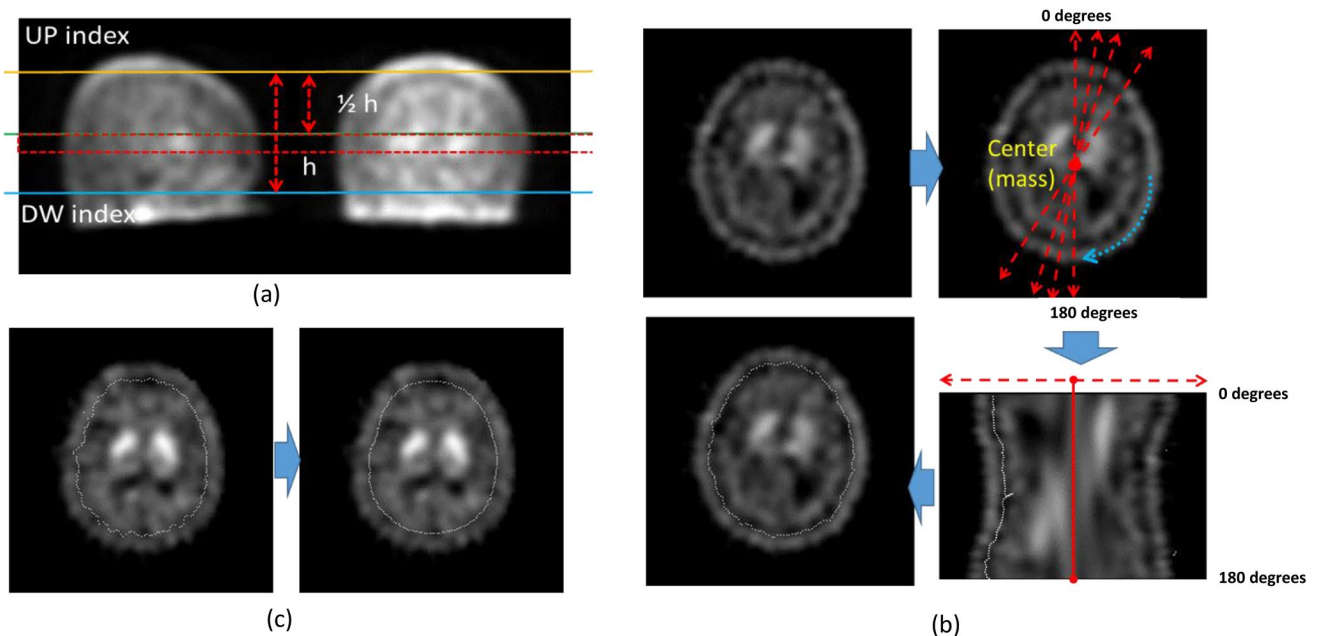
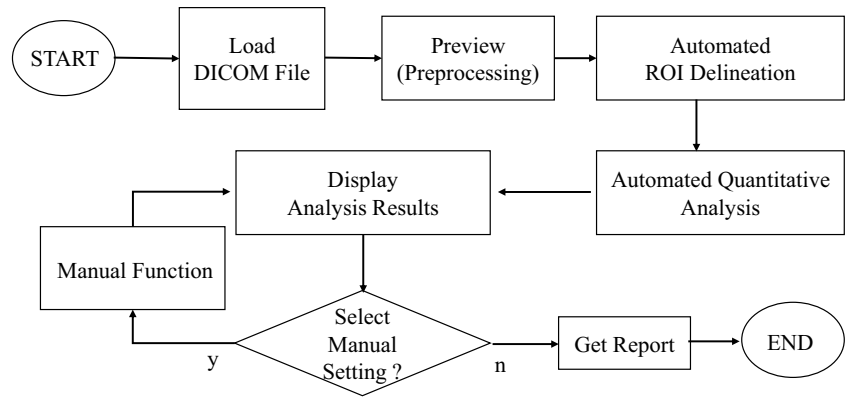


**Fig. 2** Example of brain size analysis for a subject. **a** Evaluation of striatum placement, **b** right-bottom panel showing that polar converted image from original image (top panel). The A-Star (A\*) search algorithm was used to find the shortest path from polar converted

image. Transaxial slice (left-bottom panel) showing result of brain contour obtained using line detection. **c** Brain contour after smoothing

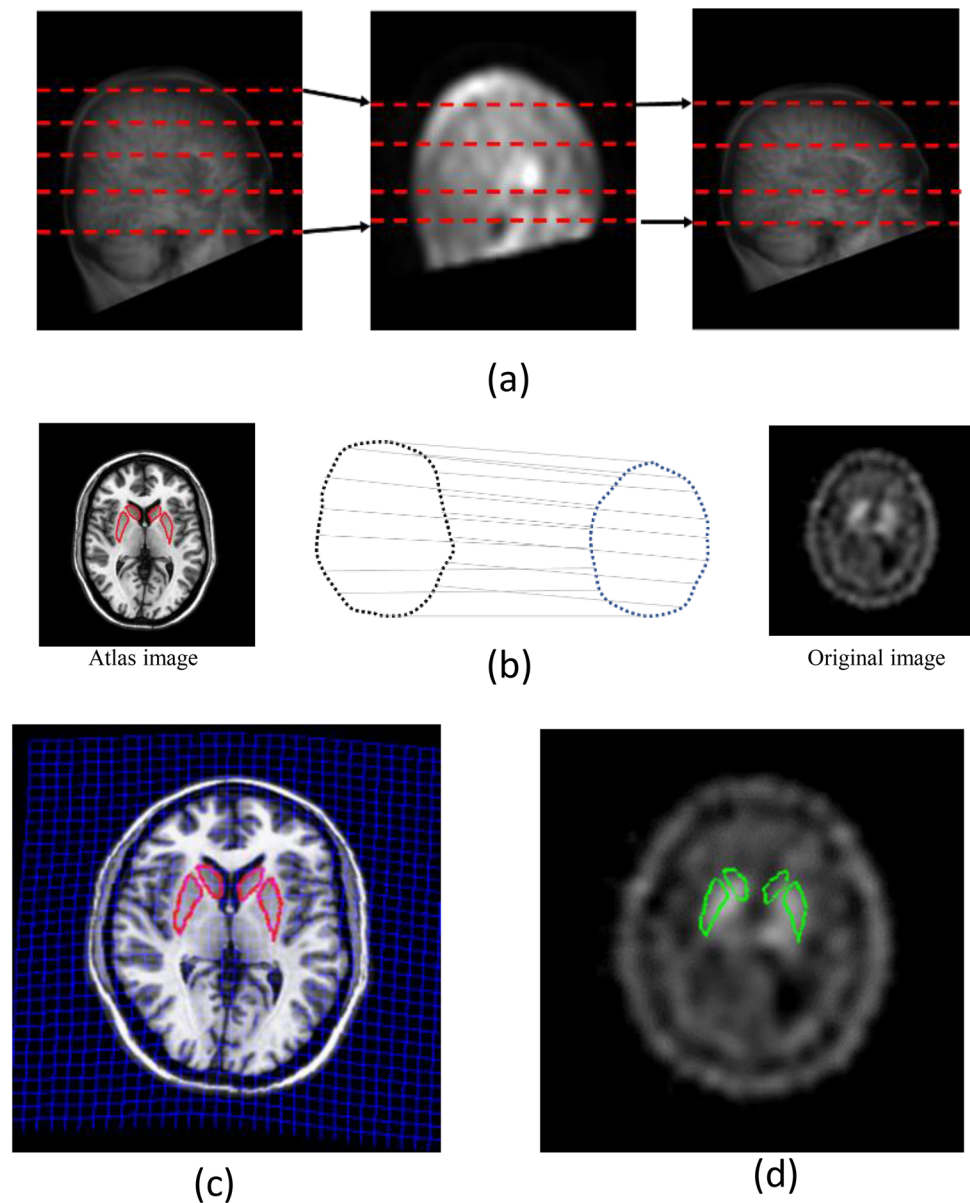
the lowest value of the lower part in the profile is detected as “DW” index. Figure 2a shows the determined parameters for the top and bottom of the brain. According to the range from the “Up” to “DW” indices, we can define the height  $h$ . The first slice ( $Str_{1st}$ ) on the volume of the striatum is obtained at the “Up” indices +  $h/2$ . The last slice on the volume of the striatum is obtained at the “Str<sub>1st</sub>” indices + 24 mm.

**2.1.1.2 Setting ROI on Brain** To get the contour of the brain along the transversal plane for each slice, images are converted from Cartesian coordinates ( $x, y$ ) to polar coordinates ( $r, \theta$ ). ( $x_0, y_0$ ) of mass of image is set as the image center of the polar coordinates. After this conversion, line detection is used to extract the boundary of the brain. Figure 2b shows

the contour of the brain detected using A-Star (A\*) search algorithm based on a conversion from polar coordinates ( $r, \theta$ ) to Cartesian coordinates ( $x, y$ ). To remove small noise, all contour lines are smoothed using a median filter, as shown in Fig. 2c.

**2.1.1.3 Setting ROI on Striatum** First, an anatomical parcelation of the spatially normalized single-subject high-resolution T1 volume provided by the Montreal Neurological Institute (MNI) [26] was employed as a normal template set, which is set up for spatial normalization of the brain. For vertical scaling of the brain, the template set is resampled using image interpolation, as shown in Fig. 3a. For horizontal warping of the brain, thin plate splines [22] are applied

**Fig. 3** Steps for setting ROI on striatum (caudate and putamen). **a** Vertical scaling atlas image based on original image. **b** Contours of brain corresponding to one transaxial slice. **c** Atlas warping. Red lines: transformed reference atlas; light blue grid: backward warp transform from atlas to original image. **d** Mapping result of ROIs of striatum



to generate warping template images based on landmarks created by the smoothed contour of the brain, as shown in Fig. 3b. After whole-brain scaling and warping of the normal template set, the warped ROIs are mapped to the striatum in the SPECT images. We also check whether the 13th slice has the maximum area of the SUR. If not, all ROIs of the striatum are moved into the slice with the maximum area of the SUR.

### 2.1.2 Quantitative Analysis

The software was developed for reconstructed and attenuation-corrected SPECT brain images. The reconstructed SPECT images are shown as a 50-slice transaxial display. All slices are resampled to a  $1\text{-mm}^3$  (image size of

$256 \times 256 \times 256$  pixels) resolution. The ROIs for the left and right striatum and the whole brain without striatum are set automatically for each subject.

Verification of the proposed method was conducted using the striatal SUR and the left–right asymmetry index. The tracer uptake value was quantified using the striatal SUR, defined as:

$$\text{SUR} = \frac{\text{Target} - \text{Reference}}{\text{Reference}} \quad (1)$$

where Target is the mean activity concentration in the striatal region (caudate or putamen) and Reference is the mean activity concentration in the reference region. In this study, the 75th percentile activity concentration of the whole brain

without striatum was used as a reference. This was done to reduce the influence of brain atrophy and infarction as well as statistical noise associated with the estimation of non-striatal uptake [23]. The percentage of the asymmetry index (%AI) was calculated as:

$$\%AI = \left| \frac{SUR_{right} - SUR_{left}}{SUR_{right} + SUR_{left}} \right| \times 2 \times 100 \quad (2)$$

where  $SUR_{right}$  and  $SUR_{left}$  are the average values of the ROI striatum on the right and left sides, respectively. As shown, asymmetry was considered to be an absolute value.

### 2.1.3 Software Implementation

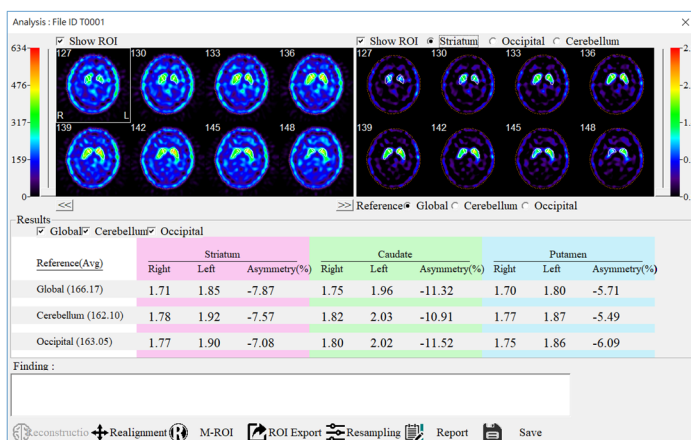
Our software was developed in C++ using Microsoft Foundation Classes (MFC), which has two solutions to implement the ROI for striatum by automatic delineation and manual

correction. This software processes, analyzes, and reports the data for  $^{99m}\text{Tc}$ -TRODAT-1 SPECT images. In Fig. 4, the software was designed for clinicians. It allows automatic striatum ROI alignment, automatic quantitative data analysis, manual ROI alignment, and manual realignment. The SUR and asymmetry index were calculated from a SPECT scan.

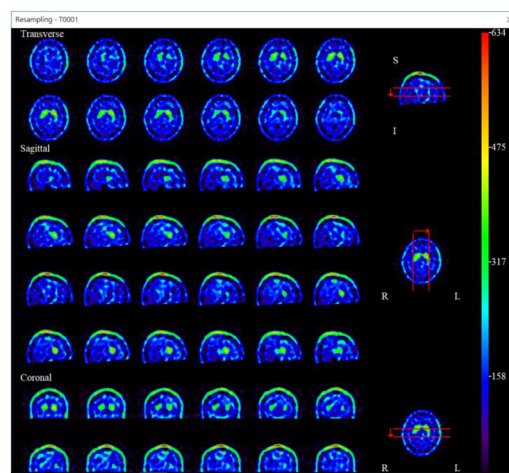
## 2.2 Manual ROI Method

### 2.2.1 Manual and MRI-Based Registration ROI Delineation

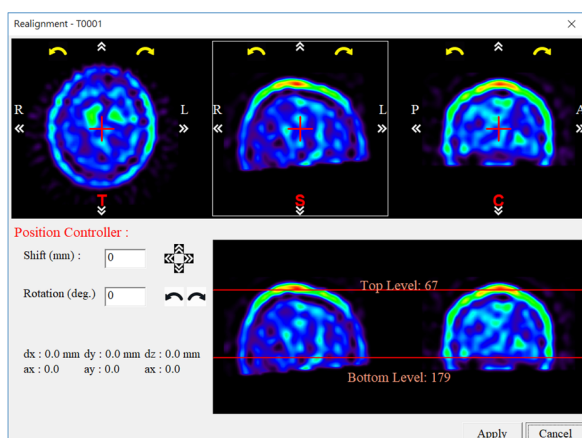
Visual inspection or manual selection of the ROI for semi-quantitative analysis is mainly used to observe and evaluate the degree of striatal defects. MRI images are considered the reference for the ROI definition of the striatum for calculating the total uptake based on ROIs. The best method for ROI delineation on the striatum is manual delineation



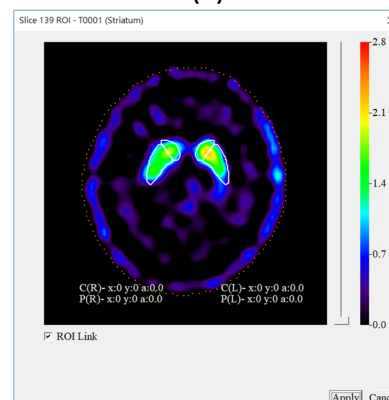
(a)



(c)



(b)



(d)

**Fig. 4** Implementing the user interface for our proposed software. **a** Main interface with automatic ROI delineation of  $^{99m}\text{Tc}$ -TRODAT-1 SPECT image for healthy volunteer, and the resulting SUR analysis (middle panel) represented as a scaled color map (upper right panel).

The corresponding interface for manual realignment (**b**) and review slices of  $^{99m}\text{Tc}$ -TRODAT-1 SPECT image (**c**). **d** The interface showing the resulting automatic ROI delineation in (**a**)

directly on SPECT images and on those based on coregistration with structural images (e.g., MRI images). In this study, MRI and SPECT images were coregistered using a manual method with visual inspection. Eight transverse slices from the SPECT images resliced with the activity uptake were selected. The manual ROI delineation on the MRI images was conducted by an experienced nuclear medicine specialist. The ROIs from MRI images were transferred to the coregistered SPECT images for semi-quantification. The average values of pixels in individual ROIs were calculated and regarded as the ground truth.

### 2.2.2 Manual ROI Delineation on SPECT Images

Because most subjects did not undergo MRI imaging, it was difficult to delineate ROIs based on only a visual inspection of the SPECT images. In addition, because SPECT images are affected by the partial volume effect, the ROIs around caudate and putamen were manually delineated directly on the SPECT slice with the highest uptake in the striatum by the same specialist.

## 2.3 Experimental Design and Test Data Collection

A total of 228 subjects (age: 19 to 90 years) who underwent a SPECT scan were included in this study. Briefly, the subjects were divided into two groups: control subjects and PD subjects. A fan-beam collimator was used for SPECT imaging. Filter back-projection (FBP) for reconstruction was used, in which a Butterworth filter was used (order = 10, cut-off = 0.46). Chang's algorithm was used for attenuation correction ( $\mu = 0.12 \text{ cm}^{-1}$ ). The image reconstruction matrix size was  $128 \times 128$  pixels. Each pixel size and the slice thickness were 3.89 mm.

To validate the performance of the proposed software, the automatic ROI delineation results were compared with those from manual delineation on SPECT images with and without the corresponding MRI images. 40 of the subjects (20 PD patients and 20 healthy controls) underwent both high-resolution T1-weighted MRI and  $^{99m}\text{Tc}$ -TRODAT-1 SPECT imaging. Figure 5 shows the estimated SURs against the true values for the 40 subjects.

For further evaluation of Parkinson's disease, the intensity ratio of striatal to non-striatal regions was calculated based on the SUR. This ratio is an important indicator for distinguishing healthy subjects from patients. 166 subjects were healthy controls, and 62 subjects were in the PD patient group. The demographics data are summarized in Table 1. The severity of PD was assessed and determined by a nuclear medicine physician using the Hoehn and Yahr scale (HYS). The study protocol was approved by Taipei Veterans General Hospital (IRB No. 2016-06-007AC) and Chung Shan Medical University Hospital (IRB No. CS19010).

## 3 Results

The main goal of this study was to develop a fully automatic ROI delineation method for computer-aided diagnosis of PD based on  $^{99m}\text{Tc}$ -TRODAT-1 brain SPECT images. We assessed whether the developed semi-quantitative analysis program is a useful aid for  $^{99m}\text{Tc}$ -TRODAT-SPECT studies in terms of creating more reproducible clinical reports.

### 3.1 Accuracy of Semi-quantitative Evaluation of TRODAT-SPECT

The proposed method was applied to 40 SPECT images. For all evaluations, each striatum was taken as an independent

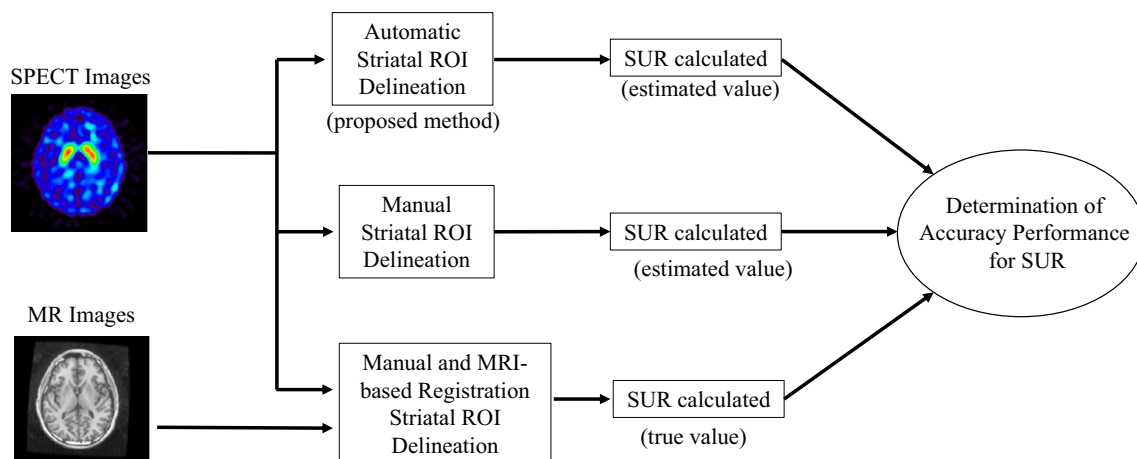


**Fig. 5** Determination of accuracy performance for SUR. True values for individual caudate and putamen were obtained using manual and MRI-based registration striatal ROI delineation. Estimated SURs were obtained using proposed method and manual method on SPECT images

**Table 1** Demographics of healthy controls and PD patients

Healthy control				PD			
Decade	Age (years)		n	HYS	Age (years)		n
	Range	Mean $\pm$ SD			Range	Mean $\pm$ SD	
20	19–25	22.6 $\pm$ 1.7	72	Stage I	51–84	64.0 $\pm$ 10.7	16
30	26–35	29.6 $\pm$ 2.8	61	Stage II	45–87	70.2 $\pm$ 10.9	34
40	36–40	38.2 $\pm$ 1.5	16	Stage III	47–84	69.8 $\pm$ 11.5	12
50	46–54	49.3 $\pm$ 2.9	9				
60	56–61	58.6 $\pm$ 2.3	8				
All	19–61	29.8 $\pm$ 9.8	166	All	45–87	68.6 $\pm$ 11.1	62

Data are presented as mean  $\pm$  standard deviation [range]

*n* number of sample cases, *HYS* Hoehn-Yahr scale, *PD* Parkinson's disease

measurement ( $n=80$ ). The SUR values for individual striatum, caudate, and putamen were obtained using three methods. Scatter plots and regression lines were used to calculate the SUR for the striatum, caudate, and putamen. The results are shown in Fig. 6. The semi-quantification of the

SUR obtained using the proposed method showed a good correlation ( $r^2=0.92$ , correlation coefficient = 0.95) with the results of delineation on the SPECT images based on coregistration with MRI images. We observed a comparable relationship in the correlation analysis ( $r^2=0.90$ , correlation

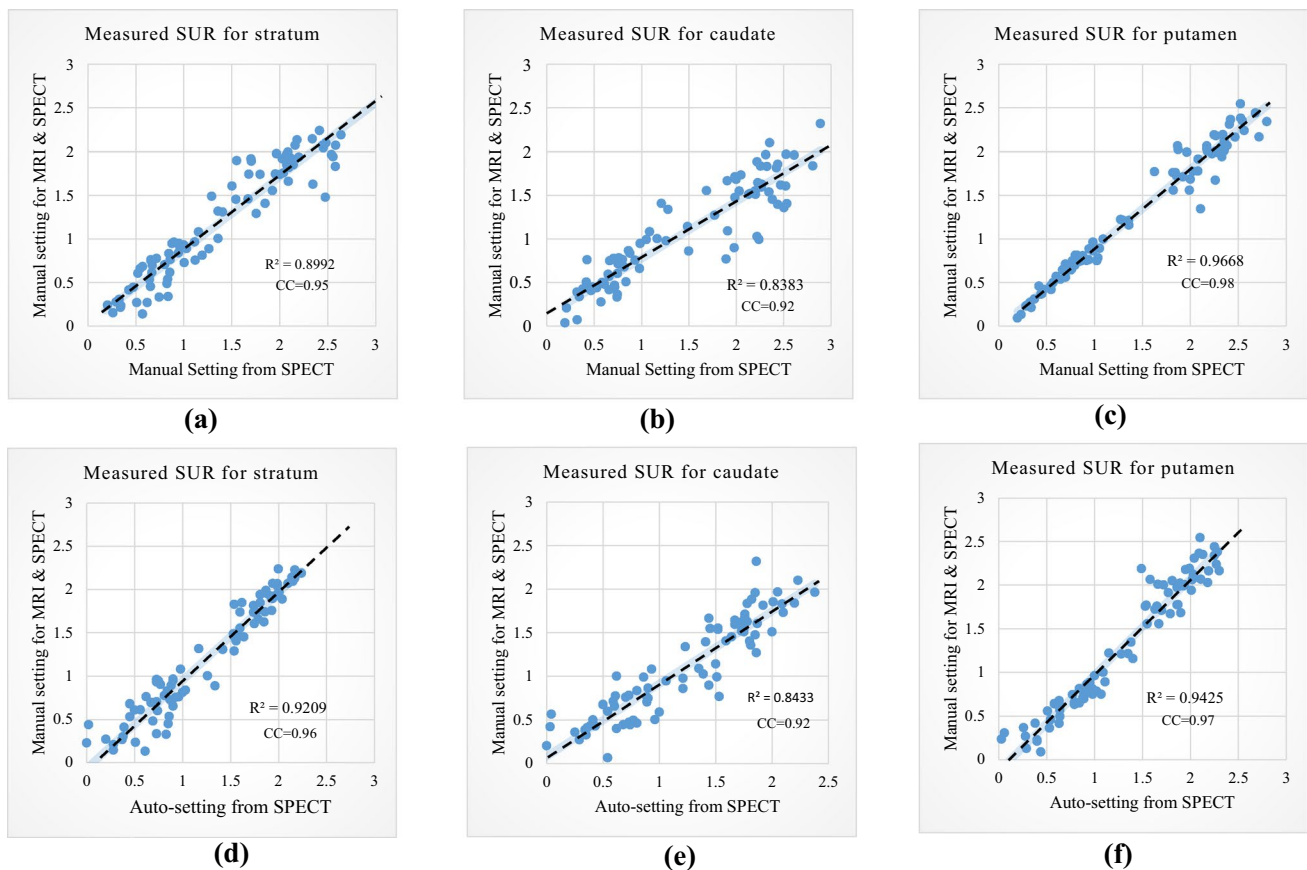


**Fig. 6** Calculated SUR values in striatum, caudate, and putamen obtained using the whole brain without striatum as the reference region against their corresponding true values. Left and right striatum of 40 subjects included as separate data points. The regression lines are shown as dashed lines. Scatterplot diagrams for the correlation

between manual setting for MRI&SPECT and manual setting from SPECT in **a** striatum, **b** caudate and **c** putamen. Scatterplot diagrams for the correlation between manual setting for MRI&SPECT and auto-setting from SPECT in **d** striatum, **e** caudate and **f** putamen

coefficient = 0.94) between the ground truth and the manually derived SUR using only one SPECT image. This indicates that our program-derived SUR values are similar to those from manual ROI delineation.

Figure 7 shows the results from the Bland–Altman analysis of the difference between the automatically evaluated SUR and the corresponding manual values against the mean of the values. For the proposed automatic method, the error was  $0.05 \pm 0.19$  in the striatum. For the manual method, the corresponding error was  $0.19 \pm 0.24$ . The SUR of the striatum was evaluated; it was found that the band of the 95% limits of agreement was slightly narrower for the proposed method compared to that for the manual method. This demonstrates that our program-derived SUR values in the striatum have the lowest variability. Specifically, SUR values were slightly overestimated by the manual method.

### 3.2 Normal Reference Values

In this study, exclusion criteria were not applied on healthy subjects to obtain normal reference ranges. With a total of 166  $^{99m}\text{Tc}$ -TRODAT-1 SPECT images selected from the 166 healthy controls, the SUR for the caudate and putamen for each individual was estimated using the proposed program. Decade-specific reference SUR values covering the ages of 19–61 years are shown in Fig. 8. As expected, the

striatal SUR values decreased with increasing age. There was no significant difference ( $p > 0.05$ ) in the SUR values between the caudate and putamen. The SUR values in the caudate and putamen correlated negatively with age (mean rate decreased with age: 3.8% per decade and 7.5% per decade, respectively). The results of our analysis confirm that the decrease in age-related SUR is higher in the putamen than in the caudate. The age-related decline of SUR availability measured in this study was 6.4% per decade for the striatum, which is consistent with results in previous studies that obtained the values manually (4 to 8%) [24].

In addition, the %AI values were calculated for all healthy subjects in order to investigate the usefulness of  $^{99m}\text{Tc}$ -TRODAT-1 imaging for the evaluation of patients with early stage PD. Because Parkinsonian syndromes tend to affect the right and left sides in the striatum with different severities, the absolute asymmetry was evaluated for the striatum. The %AI did not change with age, and thus an average reference value defined over all ages was sufficient. The values were then fitted using a linear regression line, which showed a slight increase with age. According to the age effect on SUR and %AI, two equations might be expected to whether a given subject studied in clinical practice has likely normal or abnormal values. The prediction intervals are expected to include 95% of the general population of healthy subjects to report SUR in  $[1.76 - 0.0064 \times \text{age}]$  and %AI in  $[17.5 + 0.0376 \times \text{age}]$ .

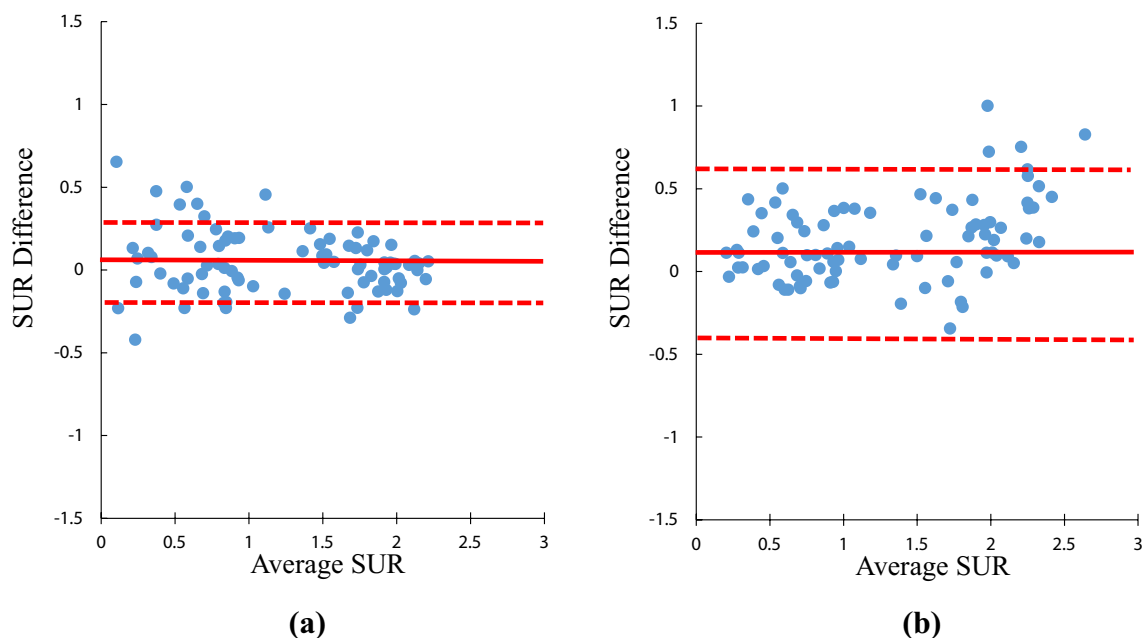


**Fig. 7** Bland–Altman plots of differences for **a** automatic ROI delineation and **b** manual ROI delineation. The mean error and the 95% limits of agreements are indicated by solid and dashed lines, respec-

tively. The whole brain without striatum was used as the reference region in all cases. The higher accuracy of the proposed automatic method was higher than that of the manual method



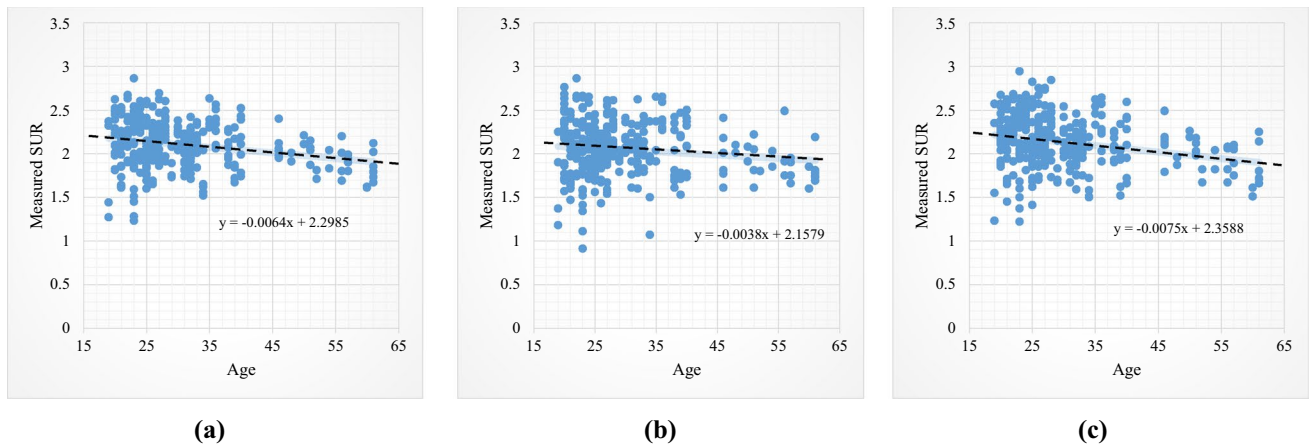


**Fig. 8** Striatal specific binding ratios versus age. Normal reference values for **a** striatum, **b** caudate, and **c** putamen. The dashed lines represent the predictions made based on the 95% confidence interval

### 3.3 Semi-quantitative Analysis for Early Parkinson's Disease

In this study, 124 striatum nuclei from 62 patients were evaluated. Figure 9 shows that the SUR and %AI values for  $^{99m}\text{Tc}$ -TRODAT-1 had a significant negative correlation with the HYS stage in the striatum. For the early PD group, 50 subjects were in the early stage of the disease (HYS stages I and II). In the SUR and %AI analysis, there was no significant difference ( $p > 0.05$ ) between PD stages I and II. However, there was a significant difference ( $p < 0.01$ ) in the

SUR and %AI between healthy controls and patients with early stage PD. The results indicate that the proposed program detected early dopaminergic changes. The SUR study indicates that our program can accurately detect the loss of dopaminergic neurons in the striatum. In the %AI study, no significant difference ( $p > 0.05$ ) was noticed among PD stages I, II, and III. In contrast to Fig. 9, the median of the %AI in the stage III PD group was higher compared with those in the early stage PD groups. However, it was difficult to distinguish severity between the groups because of a large overlap in ranges.

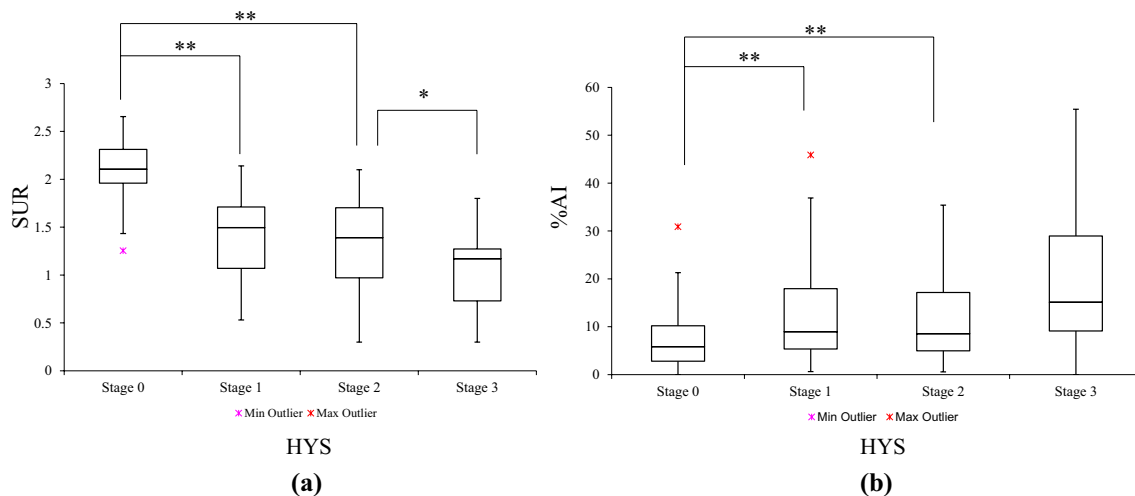


**Fig. 9** Scatterplot showing SUR values for distribution of disease severity, expressed as HYS stages. Box plot of the median striatal SUR and interquartile ranges for each subgroup are shown. **a** Analysis of variance of SUR and **b** %AI in striatum and its subre-

gions for 62 subjects with PD with HYS stages I, II, or III ( $*p < 0.05$ ,  $**p < 0.01$ , SUR striatal uptake ratio, %AI percentage of asymmetry index)

## 4 Discussion

### 4.1 Advantages of Proposed Method

Spatial normalization is a crucial step for semi-quantitative analysis software. Software such as DATquan [15], BasGan [20], and IBZM tool [21] can be used for statistical parametric mapping (SPM). However, they require a specific drug template for accurate semi-quantitative analysis [25]. For instance, the spatially normalized  $^{99m}\text{Tc}$ -TRODAT-1 images obtained from the healthy controls were averaged to be as the normal template. Some researchers have used their own MRI and SPECT templates to define the ROI. The largest difference between our automatic ROI delineation method and other automatic approaches is that SPM is not used in our approach. However, the head size of each subject must be measured to properly place a large size and fixable ROI on the caudate and putamen. For this task, striatum structures were delineated from automated anatomical labeling map [26] in a selected range of transverse slices. Figure 10 shows two examples of the automatic ROI delineation results in transaxial. Our striatal ROI included both the caudate and putamen with separating them.

Moreover, compared with manual delineation on SPECT images, the largest advantage of the proposed automatic ROI delineation approach is that it is less

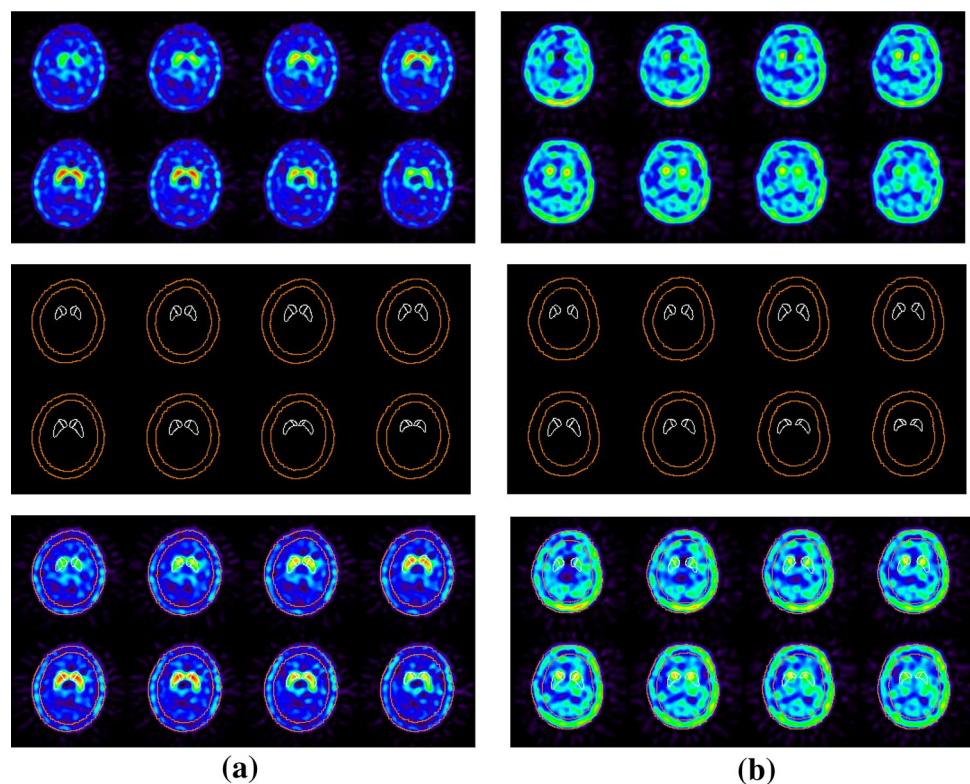
observer-dependent, requires less time, and is more reproducible. The total execution time for the SUR analysis using the proposed automatic method was around 13 s on a personal computer (1.8-GHz CPU, 8 GB of RAM, Windows 10), compared with 20–30 min required for the manual analysis method.

### 4.2 Study Limitations

There are some limitations in this study, especially the small sample size. The age of the control subjects was significantly young ( $\leq 65$  years). Hence, it is necessary to perform a large multi-center study with a large sample size to determine a highly accurate cut-off value of the  $^{99m}\text{Tc}$ -TRODAT uptake ratio for PD diagnosis.

Our results showed a slightly lower sensitivity and specificity with the use of two parameters: the SUR and %AI. We believe that this is a potential limitation of this study. We have demonstrated that there was an age-related decline of SUR measured in the healthy controls. The striatal distinction is obvious in the majority of patients with early stage PD when viewing the  $^{99m}\text{Tc}$ -TRODAT-1 images. However, the age-related decline of the SUR in the healthy controls is sometimes similar to the reduction of the SUR in patients with PD, which could reduce the diagnostic accuracy. Therefore, setting up an age-specific cutoff level is very important in clinical diagnosis in the early stage of PD.

**Fig. 10** Delineated ROIs of the right and left caudate and putamen in a selected range of transverse slices. Two examples showing a large size and fixable ROI in **a** healthy control and **b** PD. ROIs (caudate, putamen) and contours (inner and outer circles correspond to brain and head shell, respectively) overlaid on SPECT images in healthy control and PD patient



Moreover, the program requires reconstructed  $^{99m}\text{Tc}$ -TRODAT-1 SPECT images manually aligned with the anterior and posterior commissure (AC–PC) line in DICOM format. The  $^{99m}\text{Tc}$ -TRODAT-1 SPECT images of low resolution are not able to visualize AC and PC. However, the frontal lobe bottom and cerebellum tuber vermis (FLB-CTV) line is almost parallel to the AC–PC line. Therefore, axial images by the FLB-CTV line are able to create on brain SPECT images, which could be an alternative clue [27].

In our program, the ROIs of striatum were automatically delineated directly on the SPECT slices. Since TPS was used for deformable in-plane registration/warping based on only contour information. There could be a problem if the relative position of striatum is different from the normal template set. In case, we suggest that the manual function can be considered as a valid substitute to change the set of ROIs.

The program is stand-alone software for Microsoft Windows. Despite the limitations, this study found a strong correlation between the measured and true values, indicating that the proposed method could be useful for early PD diagnosis.

## 5 Conclusions

This study developed a semi-quantitative program that can perform automatic ROI delineation for semi-quantifying striatal dopamine transporter activities. Data from healthy subjects and PD patients were used to validate the accuracy and performance of the proposed program. The program is fast because neither structural information on the brain for an individual subject nor specific expertise is required. The automatic ROI delineation is more reproducible than manual delineation. The program could be a helpful tool for physicians who are inexperienced with  $^{99m}\text{Tc}$ -TRODAT-1 SPECT images. Semi-quantitative automatic analysis results can assist physicians to clinically diagnose whether a patient's neurological movement disorders are affected by dopaminergic neurodegeneration. The proposed automatic striatal ROI delineation method can be used to enhance SUR analysis in large-scale  $^{99m}\text{Tc}$ -TRODAT-1 SPECT studies.

**Acknowledgements** The authors would like to acknowledge all subjects, who patiently underwent the assessments. The authors acknowledge the financial support by the Ministry of Science and Technology of Taiwan (MOST 106-2218-E-033 -009 -MY3).

**Author Contributions** BHY and WCL designed experiments, performed research, analyzed data, contributed to discussions, and wrote the manuscript. KPL participated in design of study, investigation and the analysis of results. MFC, JHW and PFK performed experiment, collected and processed the data. RSL contributed to discussions and revised the manuscript. WCL & KPL are the guarantors of this work and, as such, had full access to all the data in the study and take

responsibility for the integrity of the data and the accuracy of the data analysis. All authors read and approved the final manuscript.

## Compliance with Ethical Standards

**Conflict of interest** The authors declare that there is no conflict of interest regarding the publication of this article.

**Ethics Approval** The study was performed following the principles outlined in the Helsinki Declaration and it was approved by the Ethics Committee (IRB Number: #2016-06-007AC and #CS19010).

## References

1. Gelb, D. J., Oliver, E., & Gilman, S. (1999). Diagnostic criteria for Parkinson disease. *Archives of Neurology*, *56*(1), 33–39. <https://doi.org/10.1001/archneur.56.1.33>.
2. Koller, W. C., Langston, J., Hubble, J., Irwin, I., Zack, M., Golbe, L., et al. (1991). Does a long preclinical period occur in Parkinson's disease? *Neurology*, *41*(52), 8–13. [https://doi.org/10.1212/WNL.41.5\\_Suppl\\_2.8](https://doi.org/10.1212/WNL.41.5_Suppl_2.8).
3. Mozley, P. D., Schneider, J. S., Acton, P. D., et al. (2000). Binding of [ $^{99m}\text{Tc}$ ] TRODAT to dopamine transporters in patients with Parkinson's disease and in healthy volunteers. *Journal of Nuclear Medicine*, *41*(4), 584–589.
4. Chou, K., Hurtig, H., Stern, M., Colcher, A., Ravina, B., Newberg, A., et al. (2004). Diagnostic accuracy of [ $^{99m}\text{Tc}$ ] TRODAT-1 SPECT imaging in early Parkinson's disease. *Parkinsonism & Related Disorders*, *10*(6), 375–379. <https://doi.org/10.1016/j.parkrel.2004.04.002>.
5. Hwang, W. J., Yao, W. J., Wey, S. P., & Ting, G. (2004). Reproducibility of  $^{99m}\text{Tc}$ -TRODAT-1 SPECT measurement of dopamine transporters in Parkinson's disease. *Journal of nuclear medicine*, *45*(2), 207–213.
6. Weng, Y.-H., Yen, T.-C., Chen, M.-C., Kao, P.-F., Tzen, K.-Y., Chen, R.-S., et al. (2004). Sensitivity and specificity of  $^{99m}\text{Tc}$ -TRODAT-1 SPECT imaging in differentiating patients with idiopathic Parkinson's disease from healthy subjects. *Journal of Nuclear Medicine*, *45*(3), 393–401.
7. Huang, W.-S., Lin, S.-Z., Lin, J.-C., Wey, S.-P., Ting, G., & Liu, R.-S. (2001). Evaluation of early-stage Parkinson's disease with  $^{99m}\text{Tc}$ -TRODAT-1 imaging. *Journal of Nuclear Medicine*, *42*(9), 1303–1308.
8. Huang, W.-S., Chiang, Y.-H., Lin, J.-C., Chou, Y.-H., Cheng, C.-Y., & Liu, R.-S. (2003). Crossover study of  $^{99m}\text{Tc}$ -TRODAT-1 SPECT and 18F-FDOPA PET in Parkinson's disease patients. *Journal of Nuclear Medicine*, *44*(7), 999–1005.
9. Ziebell, M., Pinborg, L. H., Thomsen, G., et al. (2010). MRI-guided region-of-interest delineation is comparable to manual delineation in dopamine transporter SPECT quantification in patients: A reproducibility study. *Journal of Nuclear Medicine Technology*, *38*(2), 61–68.
10. Rahmim, A., & Zaidi, H. (2008). PET versus SPECT: Strengths, limitations and challenges. *Nuclear Medicine Communications*, *29*(3), 193–207. <https://doi.org/10.1097/MNM.0b013e3282f3a515>.
11. Antonini, A., & DeNotaris, R. (2004). PET and SPECT functional imaging in Parkinson's disease. *Sleep Medicine*, *5*(2), 201–206. <https://doi.org/10.1016/j.sleep.2003.10.013>.
12. Koch, W., Radau, P. E., Hamann, C., & Tatsch, K. (2005). Clinical testing of an optimized software solution for an automated,

- observer-independent evaluation of dopamine transporter SPECT studies. *Journal of Nuclear Medicine*, 46(7), 1109–1118.
13. Mirzaei, S., Zakavi, R., Rodrigues, M., et al. (2010). Fully automated 3D basal ganglia activity measurement in dopamine transporter scintigraphy (Spectalyzer). *Annals of Nuclear Medicine*, 24(4), 295–300. <https://doi.org/10.1007/s12149-010-0353-2>.
  14. Habraken, J. B., Booij, J., Slomka, P., Sokole, E. B., & van Royen, E. A. (1999). Quantification and visualization of defects of the functional dopaminergic system using an automatic algorithm. *Journal of Nuclear Medicine*, 40(7), 1091–1097.
  15. Peter, S. J., Morten, Z., Glenna, S., et al. (2011). Validation of a method for accurate and highly reproducible quantification of brain dopamine transporter SPECT studies. *Journal of Nuclear Medicine Technology*, 39(4), 271–278. <https://doi.org/10.2967/jnmt.111.090324>.
  16. Calvini, P., et al. (2007). The basal ganglia matching tools package for striatal uptake semi-quantification: Description and validation. *European journal of nuclear medicine and molecular imaging*, 34(8), 1240–1253. <https://doi.org/10.1007/s00259-006-0357-2>.
  17. Zubal, I. G., Early, M., Yuan, O., et al. (2007). Optimized automated striatal uptake analysis applied to SPECT brain scans of Parkinson's disease patients. *Journal of Nuclear Medicine*, 48(6), 857–864. <https://doi.org/10.2967/jnumed.106.037432>.
  18. Prashanth, R., Roy, S. D., Mandal, P. K., & Ghosh, S. (2014). Automatic classification and prediction models for early Parkinson's disease diagnosis from SPECT imaging. *Expert Systems with Applications*, 41(7), 3333–3342. <https://doi.org/10.1016/j.eswa.2013.11.031>.
  19. Oliveira, F. P., Borges Faria, D., Campos Costa, D., & Tavares, J. M. (2014). A robust computational solution for automated quantification of a specific binding ratio based on [123I]FP-CIT SPECT images. *Quarterly Journal of Nuclear Medicine and Molecular Imaging*, 58(1), 74–84.
  20. Flavio, N., Mehrdad, N., Fabrizio, D. C., et al. (2013). Automatic semi-quantification of [123I]FP-CIT SPECT scans in healthy volunteers using BasGan version 2: Results from the ENC-DAT database. *European Journal of Nuclear Medicine and Molecular Imaging*, 40(4), 565–573. <https://doi.org/10.1007/s00259-012-2304-8>.
  21. Ralph, B., Georg, B., Florian, W., et al. (2006). IBZM tool: A fully automated expert system for the evaluation of IBZM SPECT studies. *European Journal of Nuclear Medicine and Molecular Imaging*, 33(9), 1073–1083. <https://doi.org/10.1007/s00259-006-0067-9>.
  22. Tsai, Y.-C., Lin, H.-D., Hu, Y.-C., et al. (2000). Thin-plate spline technique for medical image deformation. *Journal of Medical and Biological Engineering*, 20(4), 203–210.
  23. Kupitz, D., Apostolova, I., Lange, C., et al. (2014). Global scaling for semi-quantitative analysis in FP-CIT SPECT. *Nuklearmedizin*, 53(6), 234–241. <https://doi.org/10.3413/Nukmed-0659-14-04>.
  24. van Dyck, C. H., Seibyl, J. P., Malison, R. T., et al. (2002). Age-related decline in dopamine transporters: Analysis of striatal subregions, nonlinear effects, and hemispheric asymmetries. *The American Journal of Geriatric Psychiatry*, 10(1), 36–43. <https://doi.org/10.1097/00019442-200201000-00005>.
  25. Wu, C.-H., Yang, B.-H., Chou, Y.-H., et al. (2018). Effects of <sup>99m</sup>Tc-TRODAT-1 drug template on image quantitative analysis. *PLoS ONE*. <https://doi.org/10.1371/journal.pone.0194503>.
  26. Tzourio-Mazoyer, N., Landeau, B., Papathanassiou, D., et al. (2002). Automated anatomical labeling of activations in SPM using a macroscopic anatomical parcellation of the MNI MRI single-subject brain. *NeuroImage*, 15(1), 273–289. <https://doi.org/10.1006/nimg.2001.0978>.
  27. Inokuchi, Y., Koya, S., Uematsu, M., & Takashina, T. (2019). Usefulness of the frontal lobe bottom and cerebellum tuber vermis line as an alternative clue to set the axial angle parallel to the AC-PC line in I-123 IMP SPECT imaging: A retrospective study. *Radiological Physics and Technology*, 12(4), 388–392. <https://doi.org/10.1007/s12194-019-00535-5>.